AGU PUBLICATIONS

Journal of Geophysical Research: Atmospheres

Supporting Information for

Energy Budget Constraints on the Time History of Aerosol Forcing and Climate Sensitivity

C. J. Smith[1,2], G. Harris[3], M. D. Palmer[3], N. Bellouin[4], G. Myhre[5], M. Schulz[6], J.-C. Golaz[7], M. Ringer[3], T. Storelvmo[8] and P. M. Forster[1]

[1]Priestley International Centre for Climate, University of Leeds, UK. [2]International Institute for Applied Systems Analysis (IIASA), Laxenburg, Austria. [3]Met Office Hadley Centre, Exeter, UK. [4]Department of Meteorology, University of Reading, UK. [5]Center for International Climate and Environmental Research in Oslo (CICERO), Norway. [6]Norwegian Meteorological Institute, Oslo, Norway. [7]Lawrence Livermore National Laboratory, Livermore, CA, USA. [8]Department of Geosciences, University of Oslo, Norway.

Contents of this file

Text S1. Non-aerosol radiative forcing timeseries

This supplementary text describes the non-aerosol forcing time series used in the simulations. Most forcing categories are similar to those used in version 1.3 of the Finite-amplitude Impulse Response model (FaIR; Smith, Forster, et al., 2018) with updates where appropriate.

Greenhouse gases

Greenhouse gas (GHG) forcings are calculated from concentration to radiative forcing (RF) relationships (Etminan et al., 2016; Hodnebrog et al., 2013; Myhre et al., 2013). Concentrations are taken from the observationally-based CMIP6 historical time series (Meinshausen et al., 2017) extended forwards to 2020 using the SSP2-4.5 pathway (Gidden et al., 2019). To move from RF to ERF, 5% is added to the Etminan et al. (2016) RF for CO_2 and 14% subtracted from CH_4 to account for land-surface warming and tropospheric adjustments respectively (Smith, Kramer, et al., 2018). For all other GHGs, ERF is assumed to be the same as RF. We apply a 20% relative uncertainty (5-95% range) on the present-day ERF from CO_2, N_2O and other GHGs except CH_4 for which we apply 28%; this follows AR5 (Myhre et al., 2013) with an increase in the uncertainty for CH_4 following (Etminan et al., 2016). CMIP6 model results suggest these ranges are

conservative and the ERF spread is possibly lower (Smith et al., 2020). We do not modify the shape of the historical greenhouse gas forcing as historical concentrations are known with low uncertainty. This definition of greenhouse gases does not include stratospheric water vapour from methane oxidation, for which we use the Smith, Forster, et al. (2018) value of 12% of the methane ERF based on AR5.

Ozone

Historical tropospheric and stratospheric ozone forcing is used from Checa-Garcia et al. (2018) which is calculated from the CMIP6 ozone prescribed concentrations for 1850 to 2014. For extrapolating tropospheric ozone before 1850 and after 2014, we use CMIP6 historical and SSP2-4.5 precursor emissions to forcing relationships for CO, NOx, non-methane volatile organic compounds and CH_4 from Smith, Forster, et al. (2018), based on Stevenson et al. (2013), and updated coefficients to correspond to the CMIP6 emissions and Checa-Garcia et al. forcing. We use a 50% uncertainty on our best estimate of tropospheric ozone ERF of 0.36 W m^{-2} for 1750-2019. Stratospheric ozone forcing is based on equivalent effective stratospheric chlorine (EESC) of halogenated compound concentrations (Newman et al., 2007) and has a 200% relative uncertainty following AR5 around the best estimate of -0.05 W m^{-2}.

Other anthropogenic forcings

Land use forcing from Ghimire et al. (2014) is used for the historical period, scaled to -0.12 W m^{-2} for 1750-2011, and extrapolated forward using cumulative land-use CO_2 emissions to 2019 (Smith, Forster, et al., 2018). To this we apply a 75% uncertainty range. For aviation contrail forcing, we sum radiative forcing (RF) from linear contrails from Gettelman & Chen (2013) and radiative forcing from contrail cirrus from Bock & Burkhardt (2016), both based on the year 2006. This is converted to a timeseries of radiative forcing by scaling by aviation NOx emissions, using aviation NOx emissions as a proxy for aviation activity. The aviation ERF is derived from the RF by multiplying by 35% (Bickel et al., 2020) owing to strongly-opposing rapid adjustments, and is small (0.02 W m^{-2}). Black carbon on snow forcing follows BC emissions in the SSP time series and is scaled to 0.08 W m^{-2} in 2018 relative to 1750.

Volcanic forcing

Volcanic ERF is calculated using -18τ (Gregory et al., 2016), where τ is the stratospheric aerosol optical depth (SAOD) at 550 nm. We combine 3 overlapping datasets for SAOD: the eVolv database for the period 500 BCE to 1900 CE (Toohey & Sigl, 2017), the CMIP6 historical volcanic SAOD for 1850-2014, and the GloSSAC dataset for 1979-2018 (Kovilakam et al., 2020). The GloSSAC dataset is converted from SAOD at 525 nm to the target 550 nm using an Ångstrom exponent of -2.33 (Kovilakam et al., 2020). For 2019 we repeat 2018 noting no significant eruptions occurred (Global Volcanism Program, 2013). A linear transition between eVolv and CMIP6 is performed for 1850-1900 and for CMIP6 to GloSSAC for 1979-1989. The time-mean SAOD over the 2519 years of available data is defined to be the zero forcing, such that quiescent years have a small positive forcing. The rationale for this is that the long-term mean temperature anomaly should be zero when only volcanic forcing is present.

Solar forcing

The solar forcing is taken from the derived SATIRE-M ^{14}C solar irradiance database for the 9000 years up to 2014 (Vieira et al., 2011) and the concurrent CMIP6 total solar irradiance from 2015 onwards (Matthes et al., 2017). The solar irradiance timeseries is referenced to the two solar cycles spanning 1745-1765, as a proxy for 1750 conditions. Effective radiative forcing from solar variability is then calculated from the annual total solar irradiance anomaly, multiplied by ¼ (geometric effect) × 0.71 (planetary co-albedo) × 0.72 (tropospheric and stratospheric adjustments (Gray et al., 2009; Smith, Kramer, et al., 2018)).

.

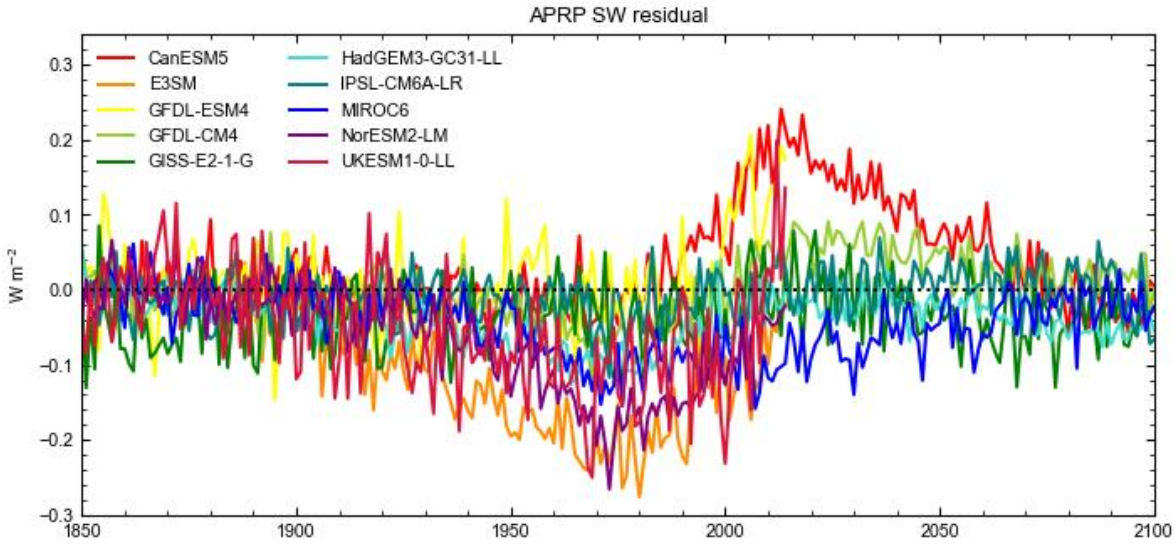

Figure S1: Residual from shortwave APRP decomposition of aerosol ERF in RFMIP and AerChemMIP models and E3SM (showing ERF_{SW} - $ERFari_{SW}$ - $ERFaci_{SW}$)

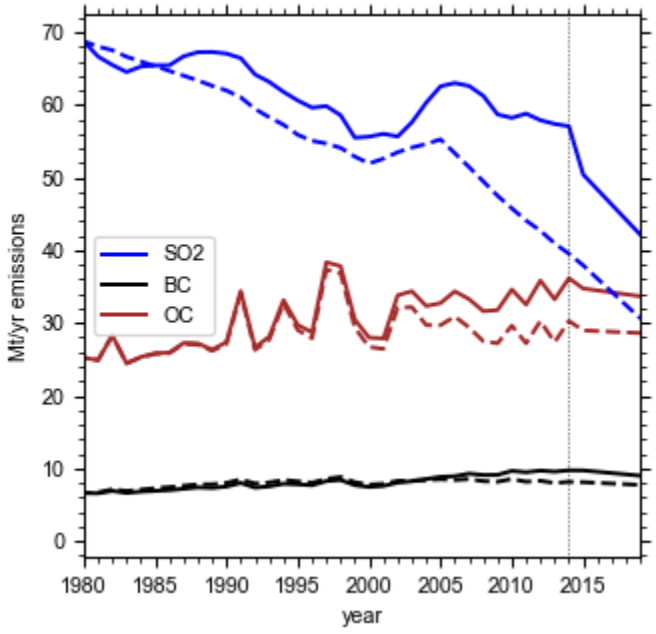

Figure S2: Comparison of the CMIP6 emissions dataset (solid lines) with the ECLIPSE v6b emissions dataset considered as an alternative in this study. Solid lines are the CMIP6 emissions, dashed lines are the ECLIPSE v6b emissions. SO_2 is expressed in Mt

S. A linear transition is performed between 1980 and 1990, which is the first year of ECLIPSE emissions.

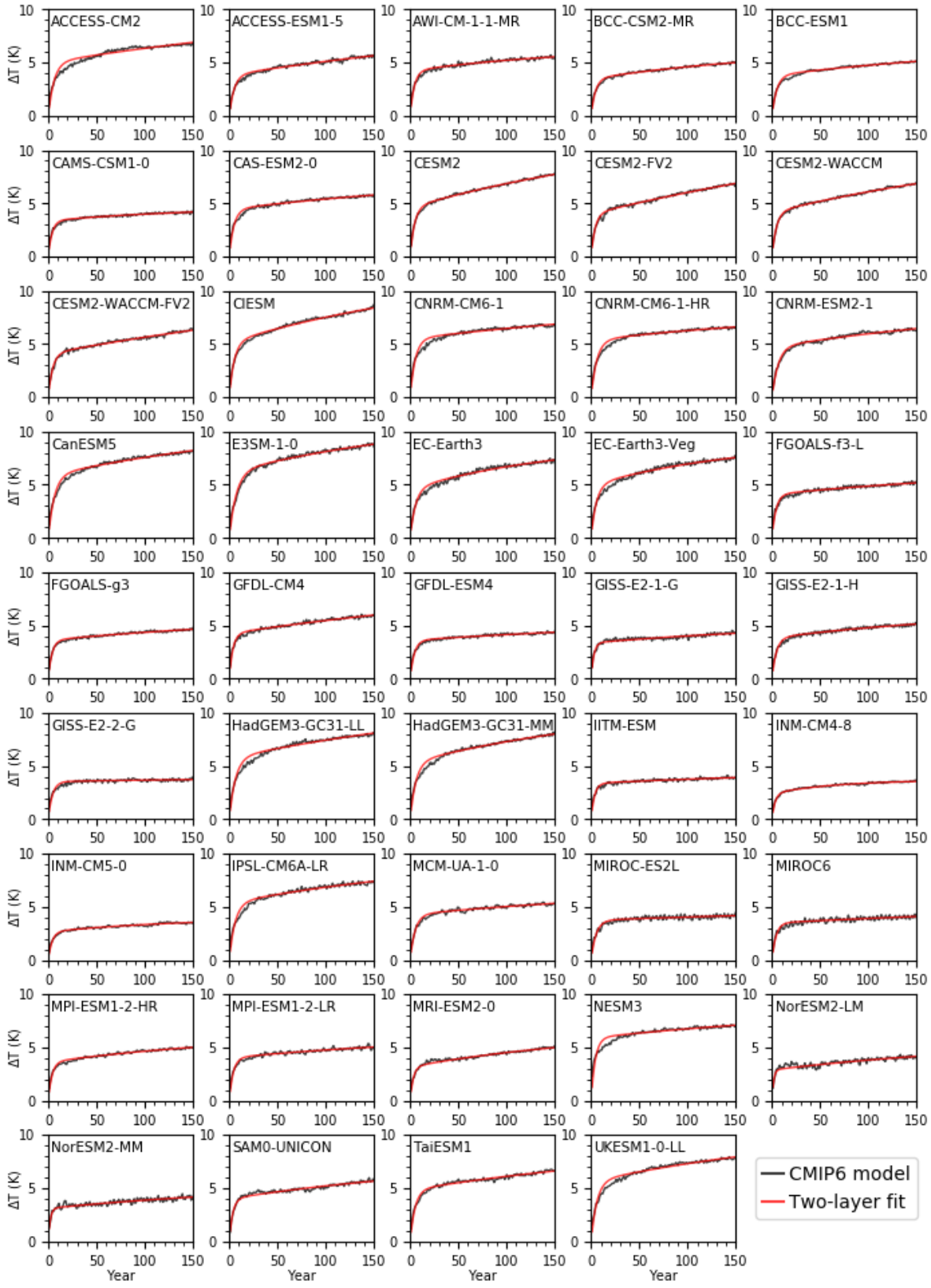
ACCESS-CM2
ACCESS-ESM1-5
AWI-CM-1-1-MR
BCC-CSM2-MR
BCC-ESM1
CAMS-CSM1-0
CAS-ESM2-0
CESM2
CESM2-FV2
CESM2-WACCM
CESM2-WACCM-FV2
CIESM
CNRM-CM6-1
CNRM-CM6-1-HR
CNRM-ESM2-1
CanESM5
E3SM-1-0
EC-Earth3
EC-Earth3-Veg
FGOALS-f3-L
FGOALS-g3
GFDL-CM4
GFDL-ESM4
GISS-E2-1-G
GISS-E2-1-H
GISS-E2-2-G
HadGEM3-GC31-LL
HadGEM3-GC31-MM
IITM-ESM
INM-CM4-8
INM-CM5-0
IPSL-CM6A-LR
MCM-UA-1-0
MIROC-ES2L
MIROC6
MPI-ESM1-2-HR
MPI-ESM1-2-LR
MRI-ESM2-0
NESM3
NorESM2-LM
NorESM2-MM
SAM0-UNICON
TaiESM1
UKESM1-0-LL
ΔT (K)
Year
CMIP6 model
Two-layer fit

109

Figure S3: Two-layer model fits to CMIP6 abrupt 4xCO_2 global surface air temperature (GSAT).

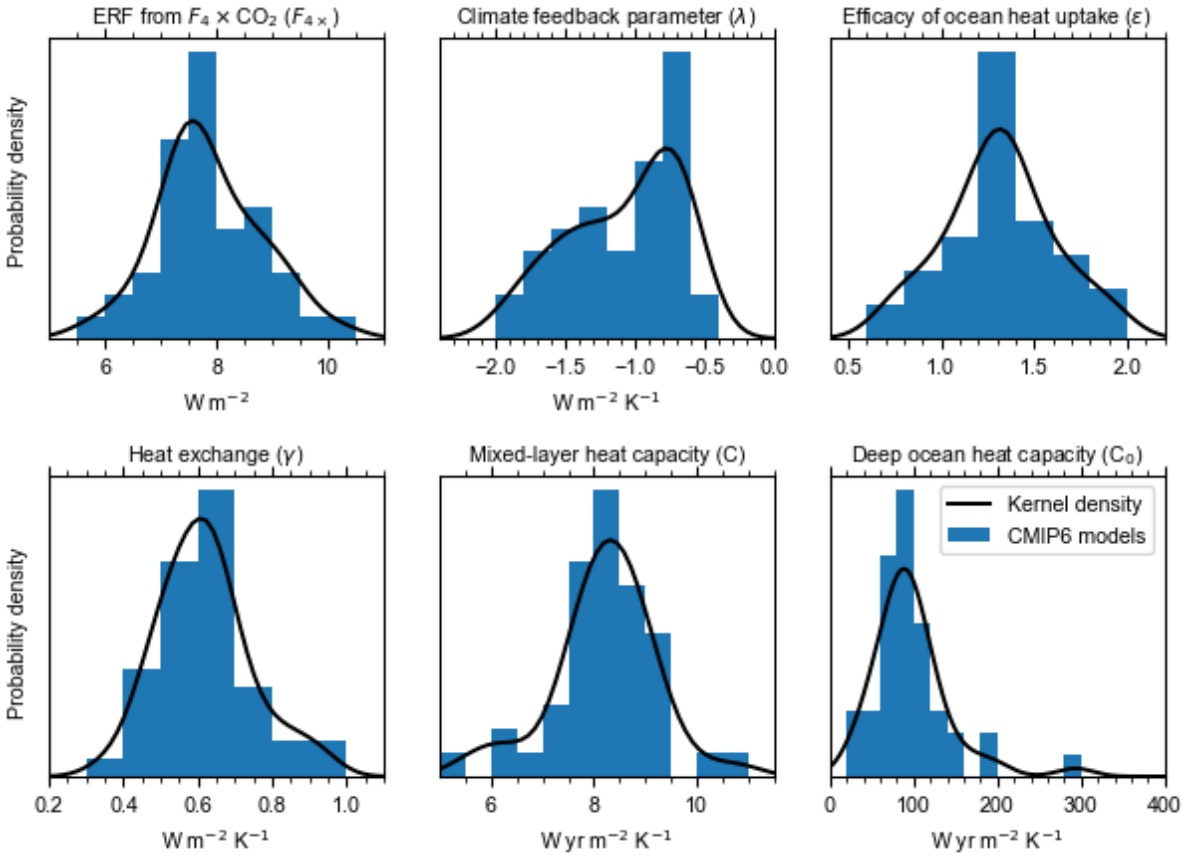

Figure S4: Histograms of Geoffroy model parameter emulations from CMIP6 model and kernel density estimate fit to distributions

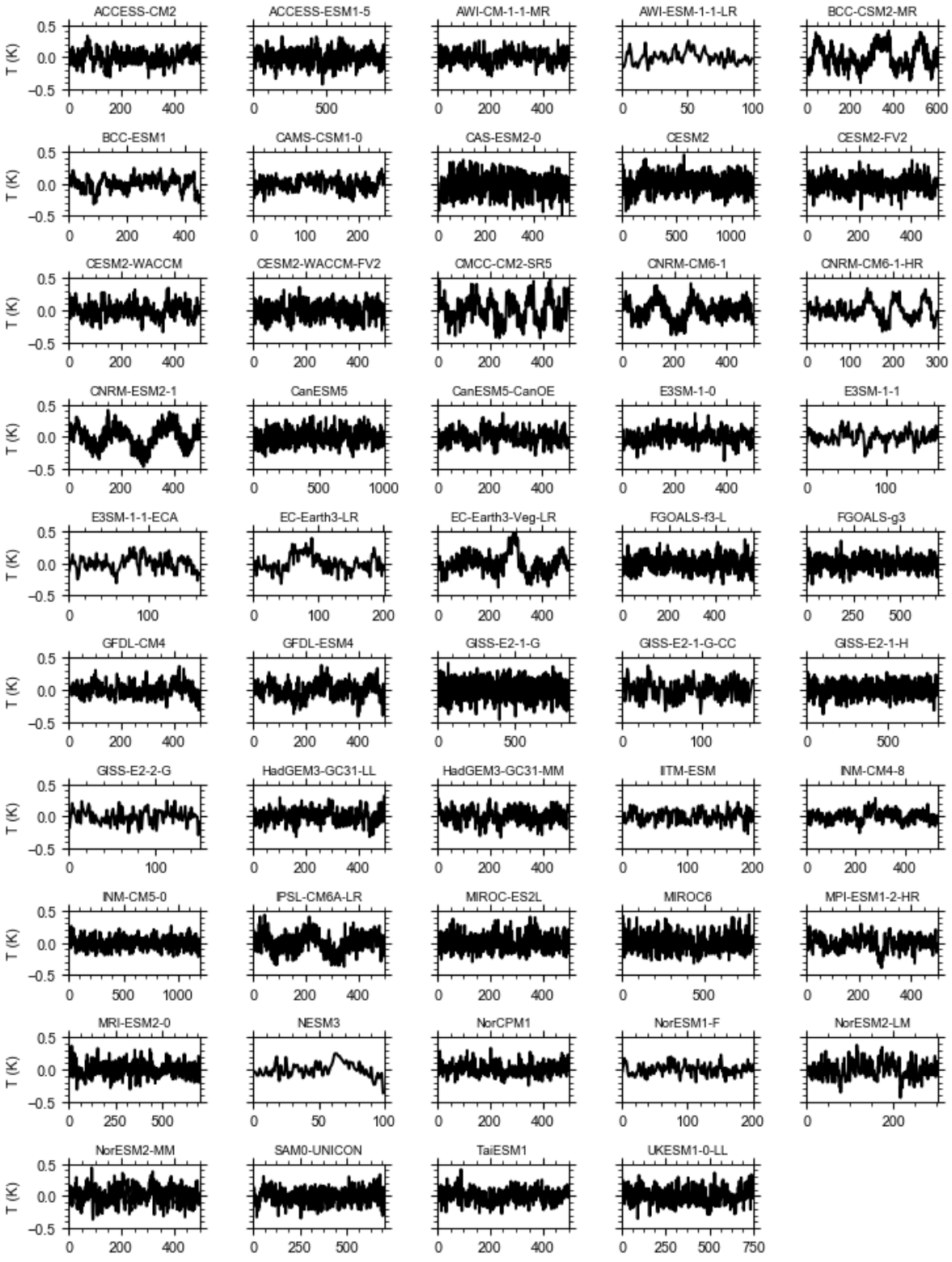

Figure S5: De-trended CMIP6 pre-industrial control global mean temperature anomalies used for characterisation of internal variability.

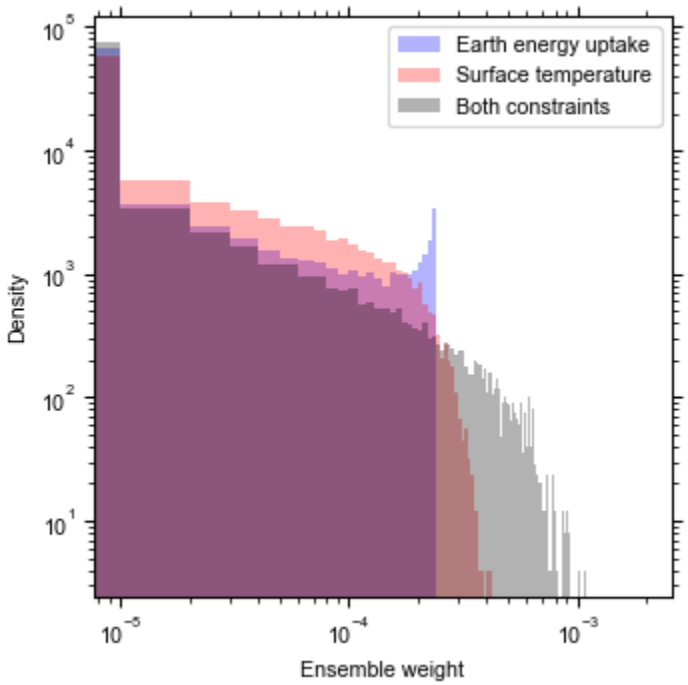

Figure S6: log-log histogram of ensemble member density using ocean heat uptake only (blue), surface temperature only (red) and both constraints (grey). Most ensemble members have a low weight and near-zero contribution to the total ensemble.

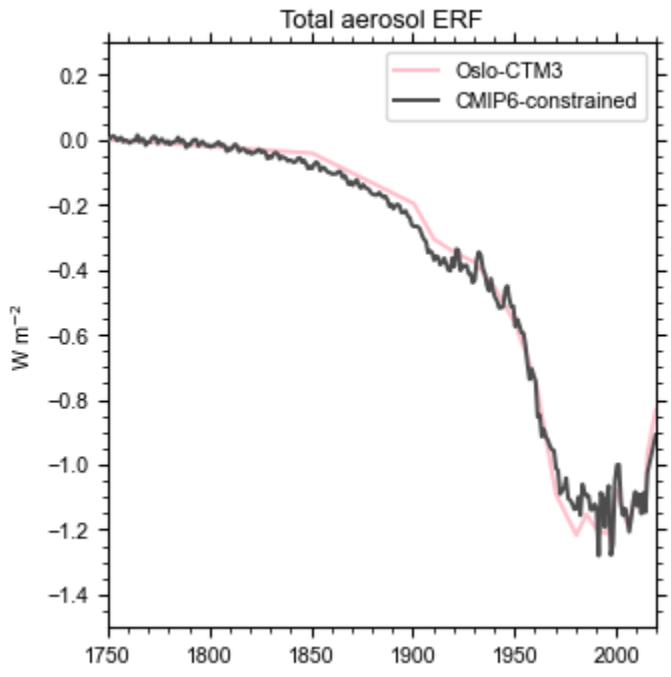

Figure S7: Comparison of best-estimate aerosol ERF from the CMIP6-constrained time-series and Lund et al., (2018, 2019) time series from Oslo-CTM3 scaled based on observational constraints.

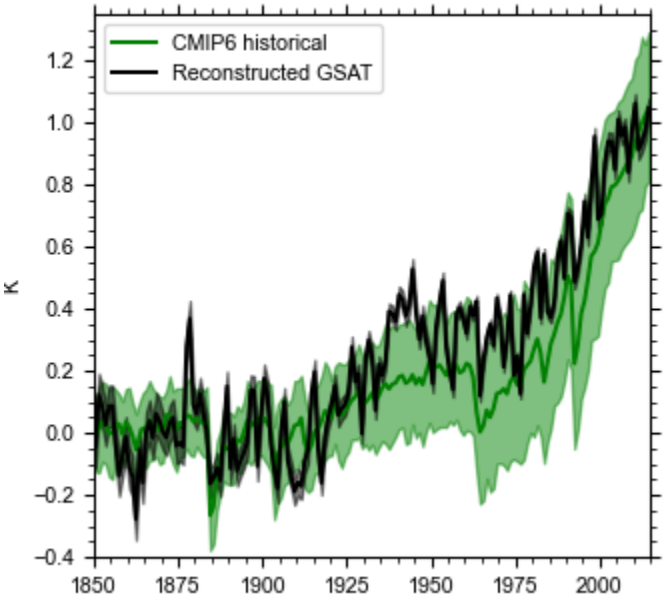

Figure S8: Historical warming simulated by 47 CMIP6 models (r1i1p1f1 used where multiple realisations exist) compared with reconstructed GSAT observations.

Table S1: Two-layer model parameter fits for CMIP6 models.

Model	F_{4x}	λ	C_{mix}	C_{deep}	γ	ε	ECS
ACCESS-CM2	7.66	-0.69	8.82	97.46	0.53	1.49	5.57
ACCESS-ESM1-5	6.97	-0.72	9.02	96.79	0.61	1.71	4.83
AWI-CM-1-1-MR	8.41	-1.30	8.17	54.70	0.49	1.30	3.24
BCC-CSM2-MR	6.89	-1.06	8.51	73.69	0.64	1.32	3.25
BCC-ESM1	6.68	-0.94	8.47	91.72	0.58	1.33	3.57
CAMS-CSM1-0	8.88	-1.88	10.01	62.41	0.53	1.34	2.37
CAS-ESM2-0	7.13	-0.93	7.57	72.83	0.45	1.43	3.84
CESM2	8.84	-0.72	8.33	70.64	0.64	1.73	6.15
CESM2-FV2	7.94	-0.56	7.96	91.10	0.70	1.91	7.10
CESM2-WACCM	8.28	-0.73	8.72	84.86	0.72	1.63	5.64
CESM2-WACCM-FV2	7.13	-0.59	7.60	111.71	0.71	1.54	6.00
CIESM	8.94	-0.72	8.59	73.23	0.67	1.38	6.25
CNRM-CM6-1	7.51	-0.77	7.05	121.14	0.56	1.03	4.88
CNRM-CM6-1-HR	7.53	-0.94	8.07	90.43	0.58	0.75	3.99
CNRM-ESM2-1	5.70	-0.63	7.48	94.94	0.61	0.87	4.51
CanESM5	7.61	-0.66	7.86	78.83	0.54	1.09	5.78

E3SM-1-0	7.42	-0.64	8.43	43.77	0.36	1.41	5.81
EC-Earth3	7.37	-0.82	8.46	38.41	0.48	1.43	4.48
EC-Earth3-Veg	7.81	-0.85	8.12	38.54	0.45	1.42	4.57
FGOALS-f3-L	9.54	-1.43	9.29	87.98	0.53	1.63	3.33
FGOALS-g3	7.87	-1.28	8.21	112.65	0.67	1.30	3.07
GFDL-CM4	8.45	-0.89	7.36	96.54	0.58	1.85	4.75
GFDL-ESM4	7.34	-1.27	8.44	129.94	0.60	1.23	2.88
GISS-E2-1-G	8.11	-1.46	6.52	145.03	0.85	1.09	2.78
GISS-E2-1-H	7.58	-1.17	8.76	83.36	0.63	1.21	3.25
GISS-E2-2-G	7.25	-1.63	8.63	293.05	0.57	0.72	2.23
HadGEM3-GC31-LL	7.46	-0.62	8.07	78.11	0.51	1.23	5.98
HadGEM3-GC31-MM	7.37	-0.67	7.85	70.75	0.61	1.07	5.53
IITM-ESM	9.25	-1.93	9.38	159.19	0.73	1.07	2.39
INM-CM4-8	6.25	-1.69	7.84	29.20	0.64	1.21	1.85
INM-CM5-0	6.35	-1.59	9.20	51.95	0.55	1.38	2.00
IPSL-CM6A-LR	7.52	-0.76	8.21	60.03	0.44	1.35	4.93
MCM-UA-1-0	7.12	-1.04	8.48	129.93	0.74	0.80	3.41
MIROC-ES2L	7.98	-1.54	10.82	199.60	0.66	0.89	2.59
MIROC6	7.73	-1.36	9.00	182.38	0.64	1.31	2.84
MPI-ESM1-2-HR	8.63	-1.34	8.89	84.13	0.66	1.49	3.23
MPI-ESM1-2-LR	9.28	-1.46	9.25	104.63	0.63	1.29	3.18
MRI-ESM2-0	8.03	-1.20	7.89	92.84	0.94	1.34	3.34
NESM3	7.72	-0.83	5.50	103.69	0.47	0.97	4.62
NorESM2-LM	10.21	-1.77	6.01	115.66	0.90	1.92	2.89
NorESM2-MM	9.39	-1.69	6.13	116.97	0.79	1.66	2.77
SAM0-UNICON	8.69	-1.14	7.67	106.86	0.82	1.21	3.83
TaiESM1	8.51	-0.92	8.72	97.26	0.63	1.27	4.64
UKESM1-0-LL	7.61	-0.68	7.77	77.15	0.54	1.14	5.57

Table S2: Correlation coefficients used for six-dimensional joint kernel density estimate for obtaining random "meta-models" derived from CMIP6 model fits.

	F_{4x}	λ	C	C_0	γ	ε
F_{4x}	1.0000	-0.4649	0.0134	0.0533	0.3159	0.4487
λ		1.0000	-0.3400	-0.3828	-0.1569	0.1990
C			1.0000	0.1686	-0.4411	-0.4355
C_0				1.0000	0.1046	-0.2542
γ					1.0000	0.2857
ε						1.0000

Table S3: Best estimates, 68% and 90% ranges for aerosol forcing, ECS and TCR from each scaled historical aerosol time series based on weighted percentiles of the distribution after applying constraints. Aerosol ERFs are for 2019 relative to 1750 and for the SSP2-4.5 scenario except for ECLIPSE-constrained.

Time series	**Variable**	**5%**	**16%**	**50%**	**84%**	**95%**

CMIP6-constrained	ECS	1.93	2.35	3.13	4.44	5.99
	TCR	1.34	1.53	1.85	2.29	2.68
	ERFaer	-1.49	-1.25	-0.89	-0.56	-0.37
	ERFari	-0.6	-0.45	-0.27	-0.14	-0.07
	ERFaci	-1.17	-0.93	-0.59	-0.29	-0.13
ECLIPSE-constrained	ECS	1.88	2.29	3.03	4.16	5.49
	TCR	1.31	1.5	1.8	2.23	2.56
	ERFaer	-1.37	-1.07	-0.72	-0.43	-0.26
	ERFari	-0.66	-0.44	-0.23	-0.1	-0.04
	ERFaci	-0.99	-0.76	-0.46	-0.21	-0.08
CanESM5	ECS	1.75	2.1	2.82	3.76	4.74
	TCR	1.23	1.42	1.72	2.12	2.39
	ERFaer	-0.89	-0.66	-0.34	-0.06	0.08
	ERFari	0.05	0.08	0.13	0.18	0.22
	ERFaci	-0.98	-0.77	-0.46	-0.21	-0.08
E3SM	ECS	1.94	2.36	3.13	4.45	5.95
	TCR	1.35	1.53	1.84	2.28	2.65
	ERFaer	-1.32	-1.18	-0.91	-0.63	-0.47
	ERFari	-0.68	-0.55	-0.38	-0.24	-0.16
	ERFaci	-0.91	-0.77	-0.51	-0.26	-0.13
GFDL-CM4	ECS	1.88	2.29	3.01	4.16	5.4
	TCR	1.3	1.5	1.8	2.21	2.51
	ERFaer	-1.04	-0.86	-0.58	-0.32	-0.18
	ERFari	-0.17	-0.14	-0.1	-0.06	-0.04
	ERFaci	-0.97	-0.77	-0.48	-0.21	-0.08
GFDL-ESM4	ECS	1.88	2.27	2.96	4.09	5.37
	TCR	1.3	1.49	1.77	2.15	2.44
	ERFaer	-1.22	-1.06	-0.76	-0.47	-0.31
	ERFari	-0.31	-0.25	-0.17	-0.11	-0.07
	ERFaci	-1.07	-0.88	-0.57	-0.29	-0.13
GISS-E2-1-G	ECS	1.97	2.42	3.23	4.71	6.38
	TCR	1.36	1.55	1.89	2.36	2.75
	ERFaer	-1.56	-1.34	-0.96	-0.58	-0.36
	ERFari	-0.26	-0.21	-0.14	-0.09	-0.06
	ERFaci	-1.43	-1.21	-0.81	-0.43	-0.21
HadGEM3-GC31-LL	ECS	1.89	2.32	3.04	4.23	5.46
	TCR	1.31	1.5	1.82	2.24	2.57
	ERFaer	-1.32	-1.15	-0.83	-0.53	-0.36
	ERFari	-0.37	-0.3	-0.2	-0.13	-0.08
	ERFaci	-1.13	-0.93	-0.61	-0.31	-0.14
IPSL-CM6A-LR	ECS	1.93	2.36	3.13	4.44	5.82
	TCR	1.34	1.53	1.85	2.3	2.66
	ERFaer	-1.2	-1.06	-0.82	-0.57	-0.42
	ERFari	-0.62	-0.49	-0.34	-0.21	-0.14
	ERFaci	-0.82	-0.69	-0.47	-0.25	-0.12

MIROC6	ECS	2	2.43	3.26	4.77	6.44
	TCR	1.38	1.56	1.89	2.36	2.75
	ERFaer	-1.48	-1.29	-0.96	-0.61	-0.41
	ERFari	-0.43	-0.35	-0.24	-0.15	-0.1
	ERFaci	-1.26	-1.06	-0.7	-0.35	-0.16
NorESM2-LM	ECS	1.93	2.36	3.12	4.41	5.86
	TCR	1.34	1.53	1.85	2.28	2.64
	ERFaer	-1.27	-1.13	-0.86	-0.58	-0.42
	ERFari	-0.57	-0.45	-0.31	-0.19	-0.13
	ERFaci	-0.96	-0.8	-0.52	-0.27	-0.12
Oslo-CTM3	ECS	1.93	2.38	3.17	4.52	6
	TCR	1.34	1.53	1.87	2.33	2.7
	ERFaer	-1.31	-1.13	-0.83	-0.54	-0.37
	ERFari	-0.43	-0.36	-0.25	-0.15	-0.1
	ERFaci	-1.09	-0.89	-0.56	-0.27	-0.11
UKESM1-0-LL	ECS	1.85	2.25	2.95	3.96	5.09
	TCR	1.29	1.48	1.78	2.17	2.46
	ERFaer	-1.1	-0.96	-0.72	-0.48	-0.34
	ERFari	-0.45	-0.36	-0.25	-0.16	-0.1
	ERFaci	-0.85	-0.7	-0.46	-0.23	-0.1

Table S4: As Table S3, using only GSAT as the constraint.

Time series	**Variable**	**5%**	**16%**	**50%**	**84%**	**95%**
CMIP6-constrained	ECS	1.95	2.36	3.15	4.57	6.11
	TCR	1.37	1.54	1.85	2.29	2.66
	ERFaer	-1.49	-1.22	-0.82	-0.48	-0.29
	ERFari	-0.6	-0.44	-0.26	-0.13	-0.06
	ERFaci	-1.15	-0.89	-0.53	-0.23	-0.08
ECLIPSE-constrained	ECS	1.94	2.34	3.11	4.42	5.86
	TCR	1.37	1.53	1.82	2.24	2.57
	ERFaer	-1.31	-1	-0.64	-0.35	-0.19
	ERFari	-0.61	-0.41	-0.21	-0.09	-0.02
	ERFaci	-0.93	-0.7	-0.4	-0.16	-0.03
CanESM5	ECS	1.91	2.31	3	4.25	5.52
	TCR	1.34	1.51	1.79	2.17	2.46
	ERFaer	-0.81	-0.58	-0.25	0.01	0.15
	ERFari	0.05	0.08	0.13	0.19	0.23
	ERFaci	-0.9	-0.68	-0.39	-0.15	-0.03
E3SM	ECS	1.93	2.34	3.11	4.49	6.02
	TCR	1.36	1.53	1.83	2.27	2.64
	ERFaer	-1.33	-1.16	-0.87	-0.58	-0.41
	ERFari	-0.66	-0.54	-0.37	-0.22	-0.14
	ERFaci	-0.91	-0.75	-0.48	-0.23	-0.09
GFDL-CM4	ECS	1.93	2.33	3.07	4.36	5.76

	TCR	1.36	1.52	1.82	2.23	2.54
	ERFaer	-1	-0.81	-0.52	-0.27	-0.13
	ERFari	-0.16	-0.14	-0.09	-0.06	-0.04
	ERFaci	-0.93	-0.72	-0.42	-0.16	-0.03
GFDL-ESM4	ECS	1.89	2.26	2.95	4.09	5.39
	TCR	1.33	1.5	1.76	2.14	2.44
	ERFaer	-1.26	-1.04	-0.7	-0.4	-0.24
	ERFari	-0.31	-0.25	-0.17	-0.1	-0.06
	ERFaci	-1.1	-0.87	-0.52	-0.23	-0.07
GISS-E2-1-G	ECS	1.96	2.38	3.21	4.69	6.37
	TCR	1.38	1.55	1.87	2.34	2.73
	ERFaer	-1.58	-1.32	-0.89	-0.49	-0.28
	ERFari	-0.26	-0.21	-0.14	-0.09	-0.05
	ERFaci	-1.45	-1.18	-0.74	-0.35	-0.13
HadGEM3-GC31-LL	ECS	1.93	2.34	3.11	4.44	5.91
	TCR	1.36	1.53	1.83	2.25	2.59
	ERFaer	-1.28	-1.09	-0.76	-0.46	-0.29
	ERFari	-0.36	-0.29	-0.2	-0.12	-0.07
	ERFaci	-1.1	-0.89	-0.55	-0.25	-0.08
IPSL-CM6A-LR	ECS	1.94	2.36	3.15	4.57	6.13
	TCR	1.37	1.54	1.85	2.3	2.68
	ERFaer	-1.18	-1.03	-0.77	-0.52	-0.36
	ERFari	-0.6	-0.48	-0.33	-0.19	-0.12
	ERFaci	-0.8	-0.66	-0.43	-0.21	-0.08
MIROC6	ECS	1.97	2.39	3.22	4.7	6.37
	TCR	1.38	1.55	1.88	2.34	2.73
	ERFaer	-1.52	-1.29	-0.9	-0.54	-0.34
	ERFari	-0.42	-0.34	-0.23	-0.14	-0.09
	ERFaci	-1.29	-1.05	-0.65	-0.3	-0.1
NorESM2-LM	ECS	1.94	2.35	3.13	4.48	5.99
	TCR	1.36	1.54	1.84	2.27	2.63
	ERFaer	-1.27	-1.1	-0.8	-0.52	-0.36
	ERFari	-0.55	-0.45	-0.3	-0.18	-0.12
	ERFaci	-0.95	-0.77	-0.48	-0.22	-0.07
Oslo-CTM3	ECS	1.96	2.39	3.2	4.62	6.24
	TCR	1.38	1.55	1.87	2.32	2.69
	ERFaer	-1.29	-1.09	-0.75	-0.46	-0.3
	ERFari	-0.43	-0.35	-0.24	-0.15	-0.1
	ERFaci	-1.07	-0.84	-0.5	-0.21	-0.06
UKESM1-0-LL	ECS	1.92	2.31	3.03	4.27	5.65
	TCR	1.35	1.51	1.8	2.2	2.51
	ERFaer	-1.06	-0.92	-0.67	-0.43	-0.29
	ERFari	-0.44	-0.36	-0.24	-0.14	-0.09
	ERFaci	-0.82	-0.66	-0.41	-0.19	-0.06

154

Table S5: As Supplementary Table 3, using only EEU as the constraint.

Time series	Variable	5%	16%	50%	84%	95%
CMIP6-constrained	ECS	2.03	2.46	3.39	5.17	7.31
	TCR	1.38	1.57	1.96	2.59	3.16
	ERFaer	-1.6	-1.34	-0.97	-0.56	-0.27
	ERFari	-0.64	-0.46	-0.27	-0.11	0.08
	ERFaci	-1.26	-1.04	-0.68	-0.32	-0.14
ECLIPSE-constrained	ECS	2.03	2.47	3.44	5.25	7.22
	TCR	1.39	1.58	1.98	2.62	3.19
	ERFaer	-1.46	-1.19	-0.82	-0.45	-0.12
	ERFari	-0.67	-0.42	-0.22	-0.05	0.32
	ERFaci	-1.13	-0.91	-0.58	-0.28	-0.12
CanESM5	ECS	1.97	2.4	3.33	5.07	7.22
	TCR	1.36	1.55	1.94	2.57	3.14
	ERFaer	-1.02	-0.81	-0.45	-0.12	0.07
	ERFari	0.08	0.12	0.2	0.29	0.36
	ERFaci	-1.18	-0.99	-0.67	-0.34	-0.15
E3SM	ECS	2.05	2.48	3.4	5.19	7.23
	TCR	1.39	1.57	1.95	2.59	3.14
	ERFaer	-1.44	-1.28	-1	-0.67	-0.47
	ERFari	-0.72	-0.58	-0.4	-0.25	-0.16
	ERFaci	-1.03	-0.85	-0.56	-0.27	-0.11
GFDL-CM4	ECS	2.06	2.5	3.47	5.37	7.5
	TCR	1.4	1.59	1.99	2.63	3.19
	ERFaer	-1.23	-1.05	-0.73	-0.42	-0.24
	ERFari	-0.2	-0.16	-0.11	-0.07	-0.05
	ERFaci	-1.13	-0.94	-0.61	-0.3	-0.12
GFDL-ESM4	ECS	2.04	2.48	3.41	5.28	7.38
	TCR	1.38	1.57	1.96	2.6	3.15
	ERFaer	-1.36	-1.19	-0.9	-0.56	-0.36
	ERFari	-0.38	-0.31	-0.21	-0.13	-0.08
	ERFaci	-1.17	-0.98	-0.67	-0.34	-0.15
GISS-E2-1-G	ECS	2.04	2.47	3.38	5.18	7.22
	TCR	1.38	1.57	1.95	2.58	3.13
	ERFaer	-1.66	-1.42	-1.02	-0.59	-0.34
	ERFari	-0.27	-0.22	-0.15	-0.09	-0.06
	ERFaci	-1.52	-1.27	-0.86	-0.43	-0.19
HadGEM3-GC31-LL	ECS	2.03	2.47	3.38	5.16	7.18
	TCR	1.38	1.57	1.95	2.59	3.14
	ERFaer	-1.6	-1.39	-1.02	-0.62	-0.39
	ERFari	-0.4	-0.32	-0.22	-0.14	-0.09
	ERFaci	-1.4	-1.17	-0.78	-0.39	-0.17
IPSL-CM6A-LR	ECS	2.05	2.48	3.39	5.17	7.19

	TCR	1.38	1.57	1.95	2.59	3.14
	ERFaer	-1.34	-1.2	-0.93	-0.61	-0.42
	ERFari	-0.61	-0.49	-0.34	-0.21	-0.14
	ERFaci	-0.99	-0.83	-0.56	-0.28	-0.12
MIROC6	ECS	2.06	2.49	3.43	5.27	7.3
	TCR	1.39	1.58	1.96	2.6	3.15
	ERFaer	-1.56	-1.35	-1	-0.62	-0.39
	ERFari	-0.44	-0.36	-0.24	-0.15	-0.1
	ERFaci	-1.34	-1.11	-0.73	-0.36	-0.15
NorESM2-LM	ECS	2.04	2.47	3.38	5.16	7.17
	TCR	1.38	1.57	1.95	2.58	3.11
	ERFaer	-1.43	-1.26	-0.97	-0.62	-0.43
	ERFari	-0.59	-0.47	-0.32	-0.2	-0.13
	ERFaci	-1.11	-0.92	-0.61	-0.3	-0.13
Oslo-CTM3	ECS	2.05	2.49	3.41	5.23	7.3
	TCR	1.39	1.58	1.96	2.59	3.14
	ERFaer	-1.44	-1.26	-0.94	-0.6	-0.39
	ERFari	-0.49	-0.39	-0.27	-0.17	-0.11
	ERFaci	-1.2	-0.98	-0.64	-0.31	-0.13
UKESM1-0-LL	ECS	2.02	2.46	3.36	5.11	7.12
	TCR	1.38	1.56	1.95	2.59	3.15
	ERFaer	-1.4	-1.23	-0.93	-0.58	-0.39
	ERFari	-0.49	-0.39	-0.27	-0.17	-0.11
	ERFaci	-1.14	-0.95	-0.63	-0.31	-0.13

References

Bickel, M., Ponater, M., Bock, L., Burkhardt, U., & Reineke, S. (2020). Estimating the Effective Radiative Forcing of Contrail Cirrus. *Journal of Climate*, *33*(5), 1991–2005. https://doi.org/10.1175/JCLI-D-19-0467.1

Bock, L., & Burkhardt, U. (2016). Reassessing properties and radiative forcing of contrail cirrus using a climate model. *Journal of Geophysical Research: Atmospheres*, *121*(16), 9717–9736. https://doi.org/10.1002/2016JD025112

Checa-Garcia, R., Hegglin, M. I., Kinnison, D., Plummer, D. A., & Shine, K. P. (2018). Historical Tropospheric and Stratospheric Ozone Radiative Forcing Using the CMIP6 Database. *Geophysical Research Letters*, *45*(7), 3264–3273. https://doi.org/10.1002/2017GL076770

Etminan, M., Myhre, G., Highwood, E. J., & Shine, K. P. (2016). Radiative forcing of carbon dioxide, methane, and nitrous oxide: A significant revision of the methane radiative forcing. *Geophysical Research Letters*, *43*(24), 12,614-12,623. https://doi.org/10.1002/2016GL071930

Gettelman, A., & Chen, C. (2013). The climate impact of aviation aerosols. *Geophysical Research Letters*, *40*(11), 2785–2789. https://doi.org/10.1002/grl.50520

Ghimire, B., Williams, C. A., Masek, J., Gao, F., Wang, Z., Schaaf, C., & He, T. (2014). Global albedo change and radiative cooling from anthropogenic land cover change,

1700 to 2005 based on MODIS, land use harmonization, radiative kernels, and reanalysis. *Geophysical Research Letters*, *41*(24), 9087–9096. https://doi.org/10.1002/2014GL061671

Gidden, M. J., Riahi, K., Smith, S. J., Fujimori, S., Luderer, G., Kriegler, E., et al. (2019). Global emissions pathways under different socioeconomic scenarios for use in CMIP6: a dataset of harmonized emissions trajectories through the end of the century. *Geoscientific Model Development*, *12*(4), 1443–1475. https://doi.org/10.5194/gmd-12-1443-2019

Global Volcanism Program. (2013). Volcanoes of the World v.4.9.0. Smithsonian Institution. https://doi.org/10.5479/si.GVP.VOTW4-2013

Gray, L. J., Rumbold, S. T., & Shine, K. P. (2009). Stratospheric Temperature and Radiative Forcing Response to 11-Year Solar Cycle Changes in Irradiance and Ozone. *Journal of the Atmospheric Sciences*, *66*(8), 2402–2417. https://doi.org/10.1175/2009JAS2866.1

Gregory, J. M., Andrews, T., Good, P., Mauritsen, T., & Forster, P. M. (2016). Small global-mean cooling due to volcanic radiative forcing. *Climate Dynamics*, *47*(12), 3979–3991. https://doi.org/10.1007/s00382-016-3055-1

Hodnebrog, Ø., Etminan, M., Fuglestvedt, J. S., Marston, G., Myhre, G., Nielsen, C. J., et al. (2013). Global warming potentials and radiative efficiencies of halocarbons and related compounds: A comprehensive review. *Reviews of Geophysics*, *51*(2), 300–378. https://doi.org/10.1002/rog.20013

Kovilakam, M., Thomason, L., Ernest, N., Rieger, L., Bourassa, A., & Millán, L. (2020). A Global Space-based Stratospheric Aerosol Climatology (Version 2.0): 1979--2018. *Earth System Science Data Discussions*, *2020*, 1–41. https://doi.org/10.5194/essd-2020-56

Matthes, K., Funke, B., Andersson, M. E., Barnard, L., Beer, J., Charbonneau, P., et al. (2017). Solar forcing for CMIP6 (v3.2). *Geoscientific Model Development*, *10*(6), 2247–2302. https://doi.org/10.5194/gmd-10-2247-2017

Meinshausen, M., Vogel, E., Nauels, A., Lorbacher, K., Meinshausen, N., Etheridge, D. M., et al. (2017). Historical greenhouse gas concentrations for climate modelling (CMIP6). *Geoscientific Model Development*, *10*(5), 2057–2116. https://doi.org/10.5194/gmd-10-2057-2017

Myhre, G., Shindell, D., Bréon, F.-M., Collins, W., Fuglestvedt, J., Huang, J., et al. (2013). Anthropogenic and Natural Radiative Forcing. In Intergovernmental Panel on Climate Change (Ed.), *Climate Change 2013 - The Physical Science Basis* (pp. 659–740). Cambridge: Cambridge University Press. https://doi.org/10.1017/CBO9781107415324.018

Newman, P. A., Daniel, J. S., Waugh, D. W., & Nash, E. R. (2007). A new formulation of equivalent effective stratospheric chlorine (EESC). *Atmospheric Chemistry and Physics*, *7*(17), 4537–4552. https://doi.org/10.5194/acp-7-4537-2007

Smith, C. J., Forster, P. M., Allen, M., Leach, N., Millar, R. J., Passerello, G. A., & Regayre, L. A. (2018). FAIR v1.3: a simple emissions-based impulse response and carbon cycle model. *Geoscientific Model Development*, *11*(6), 2273–2297. https://doi.org/10.5194/gmd-11-2273-2018

Smith, C. J., Kramer, R. J., Myhre, G., Forster, P. M., Soden, B. J., Andrews, T., et al. (2018). Understanding Rapid Adjustments to Diverse Forcing Agents. *Geophysical*

Research Letters, *45*(21), 12,023-12,031. https://doi.org/10.1029/2018GL079826
Smith, C. J., Kramer, R. J., Myhre, G., Alterskjær, K., Collins, W., Sima, A., et al. (2020). Effective radiative forcing and adjustments in CMIP6 models. *Atmospheric Chemistry and Physics Discussions*, *2020*, 1–37. https://doi.org/10.5194/acp-2019-1212
Stevenson, D. S., Young, P. J., Naik, V., Lamarque, J.-F., Shindell, D. T., Voulgarakis, A., et al. (2013). Tropospheric ozone changes, radiative forcing and attribution to emissions in the Atmospheric Chemistry and Climate Model Intercomparison Project (ACCMIP). *Atmospheric Chemistry and Physics*, *13*(6), 3063–3085. https://doi.org/10.5194/acp-13-3063-2013
Toohey, M., & Sigl, M. (2017). Volcanic stratospheric sulfur injections and aerosol optical depth from 500 BCE to 1900 CE. *Earth System Science Data*, *9*(2), 809–831. https://doi.org/10.5194/essd-9-809-2017
Vieira, L. E. A., Solanki, S. K., Krivova, N. A., & Usoskin, I. (2011). Evolution of the solar irradiance during the Holocene. *Astronomy & Astrophysics*, *531*, A6. https://doi.org/10.1051/0004-6361/201015843